Cross-analysis of magnetic and current density field topologies using experimental data in a Quiescent H-mode tokamak discharge

Marie-Christine A Firpo

Cross-analysis of magnetic and current density field topologies using experimental data in a Quiescent H-mode tokamak discharge

Marie-Christine A. Firpo
Laboratoire de Physique des Plasmas (LPP), CNRS, Sorbonne Université, Ecole polytechnique, Institut Polytechnique de Paris, 91120 Palaiseau, France

Under review, 26 August 2024

Abstract
In axisymmetric fusion devices, such as tokamaks, the winding of the magnetic field is characterized by the safety profile $q = q_{\mathbf{B}}$. Similarly, the winding of the current density field can be characterized by $q_{\mathbf{J}}$. Currently, the study of the relationship between the $q_{\mathbf{B}}$ and $q_{\mathbf{J}}$ profiles in relation to the confinement properties of tokamak plasmas remains unexplored, as the $q_{\mathbf{J}}$ profile is neither computed nor considered. Here some reconstruction of the current density winding profile is presented from experimental data in the Quiescent H-mode. The $(q_{\mathbf{B}}, q_{\mathbf{J}})$-derived topology analysis indicates a large central plasma region unaffected by current filamentation-driven resonant magnetic perturbations, while the outer region harbors a spectrum of such current filament-induced magnetic resonant modes that degrade peripheral confinement. The results suggest a QH-mode signature pattern requiring further reinforcement by additional data. Implementing $(q_{\mathbf{B}}, q_{\mathbf{J}})$ real-time monitoring could uncover insights into tokamak confinement regimes with important implications.

1 Introduction

It has been shown [1] that, in axisymmetric driven devices for fusion applications, such as the tokamak, both the magnetic and the current density fields have rotational transforms which allows a complete classification of modes according to their topology. At each given time, one can characterize the way the axisymmetric vector fields wind about the central axis through the well-known safety profile $q = q_{\mathbf{B}}$ for the magnetic field and its analogous $q_{\mathbf{J}}$ profile for the current density field or, equivalently, through their inverse functions that are traditionally named winding profiles. In the experiments, sophisticated codes resolve nowadays the Grad-Shafranov equation in real time and reconstruct the equilibrium using the data coming from the diagnostics [2–20]. This allows in particular to obtain $q_{\mathbf{B}}$ in real time. Complementing this reconstruction with the computation of $q_{\mathbf{J}}$ would offer a complete identification of the nature of the perturbation modes and unveil the turbulence actuators. Indeed, as in neutral fluids, it is an empirical fact that vorticity filaments support (velocity) turbulence [21], one may infer that current density filaments play a similar role in small-scale magnetic turbulence, that is the backbone of anomalous heat transport [22–24]. They have been extensively reported in expriments, e.g. in Refs. [25–32].

Currently, the study of the relationship between the $q_{\mathbf{B}}$ and $q_{\mathbf{J}}$ profiles in relation to the confinement properties of tokamak plasmas is a blank slate, as the $q_{\mathbf{J}}$ profile is neither computed nor taken into account. It is the objective of the present Letter to perform the first cross-analysis of the magnetic and current density field topologies. This will be done using the data of Pankin and coworkers [33] on the discharge 163518 from the DIII-D tokamak operating in the Quiescent H-mode. Quiescent H-modes, also known as QH-modes, form an operational regime in tokamak plasmas that has garnered significant attention in the magnetic confinement fusion community. This has been achieved in tokamaks with advanced plasma control systems, which allow for precise control of the plasma shape, density, and temperature. QH mode was originally discovered on DIII-D [34, 35] and was subsequently investigated on ASDEX-Upgrade [36–38], JT-60U [39, 40] and JET [37]. QH modes form a subset of high (H) confinement-mode plasmas that exhibit a unique behavior as they operate at high confinement levels without the presence of large Edge-Localized Modes (ELMs).

2 Methods

2.1 Reconstruction problem formulation

To my knowledge, the work [1] contains the first evaluation of $q_{\mathbf{J}}$ in the convenient flux coordinates. Using the Grad-Shafranov equation, the expression of the $q_{\mathbf{J}}$ profile in the usual flux function variable is [1]

$$q_{\mathbf{J}} = q_{\mathbf{B}} \left(1 + \frac{\mu_0}{\langle R^{-2} \rangle} \frac{p'(\psi)}{FF'(\psi)} \right) \tag{1}$$

where p is the pressure and F is the diamagnetic function, $F \equiv RB_\varphi$. Consequently, any classical equilibrium reconstruction code could freely add the evaluation line (1) to compute $q_{\mathbf{J}}$, as all the required information is known. Indeed, it should have converged to unfold the flux functions $p'(\psi)$ and $FF'(\psi)$ determined by minimizing the χ^2 from the measured data and have obtained $q_{\mathbf{B}}$ from

$$q_{\mathbf{B}} = \frac{F}{4\pi^2}\left\langle R^{-2}\right\rangle v'(\psi), \tag{2}$$

where v is the volume enclosed by the flux surface. Therefore it should have already computed the surface average function $\left\langle R^{-2}\right\rangle$. Our objective here is to compute $q_{\mathbf{J}}$ using the expression (1). The Figure 2 of Pankin's and coworkers article [33] represents the flux surfaces computed with EFIT for the DIII-D discharge 163518 at 2350 ms. Also plotted are the total plasma pressure, the pressure gradient p', and the FF' and $q_{\mathbf{B}}$ profiles as functions of the normalized toroidal flux. Consequently, only the data for $\left\langle R^{-2}\right\rangle$ as a function of the normalized toroidal flux is missing, and it needs to be estimated in order to use Eq. (1).

2.2 Evaluation of the flux surface averages

We use here the usual flux coordinates $\left(\psi, \theta_g, \varphi_g\right)$, where θ_g and φ_g are respectively the poloidal and toroidal geometrical angles. Let us remind the definition of the flux surface average as

$$\langle X\rangle \doteq \left(\oint_\psi \frac{d\theta'_g}{\mathbf{B}.\nabla\theta'_g}\right)^{-1} \oint_\psi \frac{X d\theta'_g}{\mathbf{B}.\nabla\theta'_g} = \frac{\partial}{\partial v}\int_V X dv'. \tag{3}$$

Using the expression of the poloidal magnetic field, this yields

$$\langle R^\alpha\rangle_{\psi=\psi_0} = \frac{\oint_{\psi=\psi_0} R^{\alpha+1}\frac{dl}{\|\nabla\psi\|}}{\oint_{\psi=\psi_0} R\frac{dl}{\|\nabla\psi\|}}. \tag{4}$$

The closed line integrals are here evaluated using [41], for any point function f,

$$\oint_{\psi=\psi_0} f(P)\frac{dl}{\|\nabla\psi\|} = \frac{d}{d\psi_0}\left(\int_{S(\psi_0)} f(P)ds\right), \tag{5}$$

where $S(\psi)$ denotes the area of the surface of the poloidal cross-section enclosed by the flux surface ψ. We have therefore

$$\langle R^\alpha\rangle(\psi_0) = \frac{\frac{d}{d\psi_0}\left(\int_{S(\psi_0)} R^{\alpha+1}ds\right)}{\frac{d}{d\psi_0}\left(\int_{S(\psi_0)} Rds\right)}. \tag{6}$$

It is possible to use in the above expression the normalized magnetic flux, ψ_N, instead of the magnetic flux. The connection with ρ is then made using the expression of ψ_N as

$$\psi_N(\rho) = \frac{\int_0^\rho \frac{s}{q_{\mathbf{B}}(s)}ds}{\int_0^1 \frac{s}{q_{\mathbf{B}}(s)}ds}. \tag{7}$$

3 Results

3.1 Computation of flux surface averages

The plasma domain has been extracted and digitized from the Fig. 2 of Ref. [33]. The last closed flux surface is the inner bold curve of Fig. 1. In order to compute the flux surface averages of R^{-2} using Eq. (6), one needs to know the flux contours. To achieve this, the Grad-Shafranov equation has been solved using this last closed flux surface as the boundary of the computational domain. Figure 1 depicts the obtained approximation of the flux contours and the red dot reports the location of the magnetic axis obtained from the Fig. 2 of Ref. [33]. One can then proceed to the evaluation of the flux surface averages of R^{-2}. The resulting estimates are depicted in Figure 2. To account for some inevitable imprecision, a confidence band is drawn around the estimated curve, spanning values between 0.93 and 1.07 times the estimated $\left\langle R^{-2}\right\rangle$.

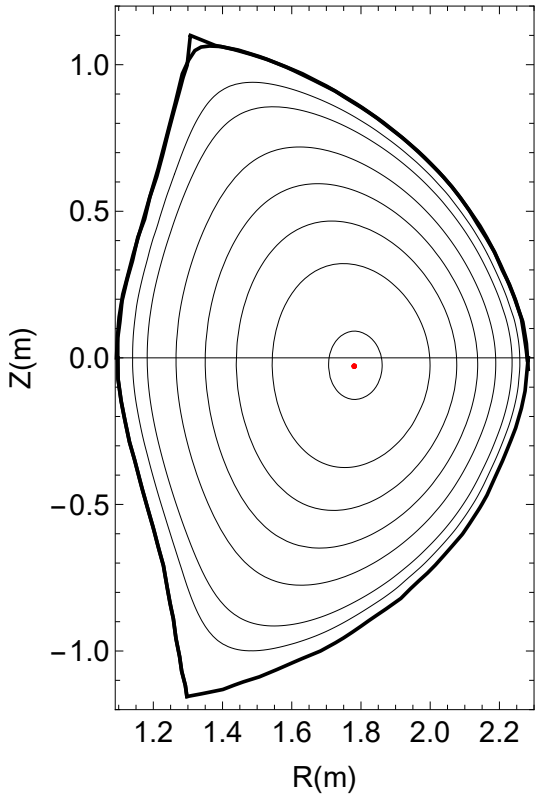

Figure 1: Reconstruction of the magnetic flux contours. The red dot stands for the magnetic axis.

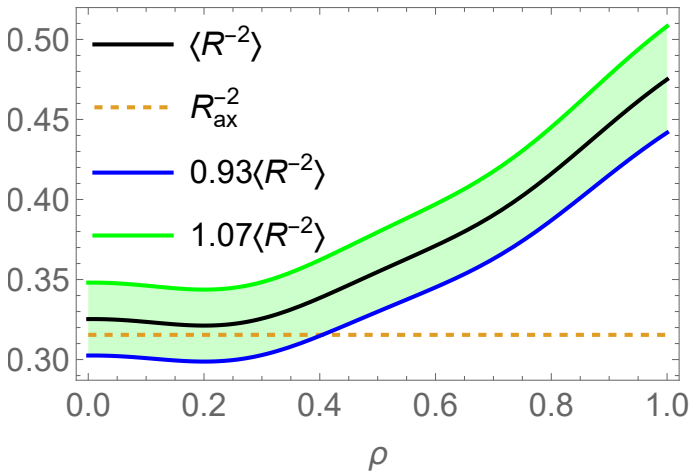

Figure 2: Evaluation of the flux surface average $\left\langle R^{-2}\right\rangle$ as a function of ρ. At $\rho = 0$, the flux surface average of R^{-2} should be R_{ax}^{-2} with R_{ax} the radius of the magnetic axis. The reconstructed curve shows some discrepancy compared to this value in the limit $\rho \to 0$. To account for some inevitable imprecision, a confidence band is shown around the estimated curve, spanning values between 0.93 and 1.07 times the estimated $\left\langle R^{-2}\right\rangle$.

3.2 Equilibrium reconstruction of the $q_{\mathbf{J}}$-profile

We have then all the requested information to compute the winding profile, $q_{\mathbf{J}}^{-1}$, of the current density field lines. The reconstructed $q_{\mathbf{J}}^{-1}$ profile is shown on Figure 3. Figure 3 represents the confidence band introduced by some uncertainty in

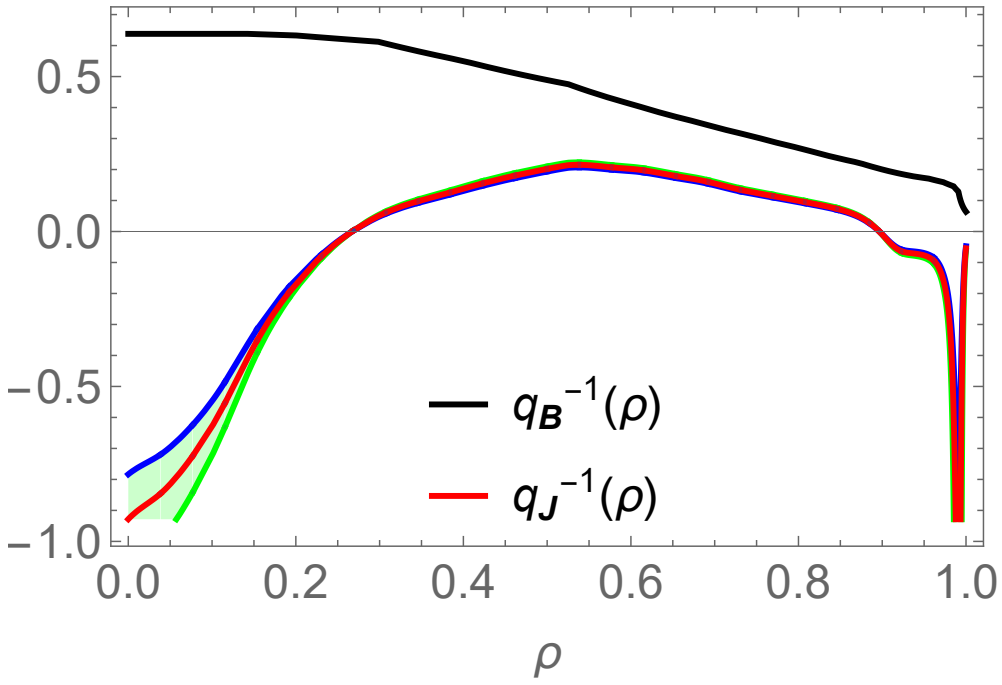

Figure 3: Evaluation of the winding profile, $q_{\mathbf{J}}^{-1}$, of the current density field lines in the QH mode. To account for some inevitable imprecision, the confidence band is depicted around the estimated curve using, in the evaluation of $q_{\mathbf{J}}^{-1}$, values spanning between 0.93 and 1.07 times the estimated $\left\langle R^{-2}\right\rangle$. The winding profile, $q_{\mathbf{B}}^{-1}$, of the magnetic field lines is represented for comparison. We do not take into account here the imprecision in the digitization of the $q_{\mathbf{B}}$, p' and FF' profiles.

the evaluation of the flux surface averages of R^{-2}. To be thoroughly rigorous, we must additionally test the robustness of the computation of $q_{\mathbf{J}}$ against errors in curve digitization. Let us then estimate the uncertainty in the evaluation of $q_{\mathbf{J}}$ introduced by digitization of the data. Considering $q_{\mathbf{J}}$ as a function of $q_{\mathbf{B}}$, $\left\langle R^{-2}\right\rangle$, p' and FF', the Laplace-Gauss uncertainty propagation formula yields, for the uncertainty on $q_{\mathbf{J}}$,

$$\begin{aligned}\Delta q_{\mathbf{J}} &= \left[\left(\frac{\partial q_{\mathbf{J}}}{\partial q_{\mathbf{B}}}\Delta q_{\mathbf{B}}\right)^2+\left(\frac{\partial q_{\mathbf{J}}}{\partial\left\langle R^{-2}\right\rangle}\Delta\left\langle R^{-2}\right\rangle\right)^2\right.\\ &\quad\left.+\left(\frac{\partial q_{\mathbf{J}}}{\partial p'}\Delta p'\right)^2+\left(\frac{\partial q_{\mathbf{J}}}{\partial FF'}\Delta FF'\right)^2\right]^{1/2}.\end{aligned}$$

After some calculations using Eq. (1), this gives

$$\begin{aligned}&\left(\frac{\Delta q_{\mathbf{J}}}{q_{\mathbf{J}}}\right)^2-\left(\frac{\Delta q_{\mathbf{B}}}{q_{\mathbf{B}}}\right)^2\\ &=\left(1-\frac{q_{\mathbf{B}}}{q_{\mathbf{J}}}\right)^2\left[\left(\frac{\Delta\left\langle R^{-2}\right\rangle}{\left\langle R^{-2}\right\rangle}\right)^2+\left(\frac{\Delta p'}{p'}\right)^2+\left(\frac{\Delta FF'}{FF'}\right)^2\right].\end{aligned}$$

Assuming that all the uncertainties are similar with $\Delta q_{\mathbf{B}}/q_{\mathbf{B}}=\Delta\left\langle R^{-2}\right\rangle/\left\langle R^{-2}\right\rangle=\Delta p'/p'=\Delta FF'/FF'=\delta$ yields

$$\frac{\Delta q_{\mathbf{J}}}{q_{\mathbf{J}}}=\delta\left[1+3\left(1-\frac{q_{\mathbf{B}}}{q_{\mathbf{J}}}\right)^2\right]^{1/2}. \tag{8}$$

For $\delta = 0.04$, one computes the uncertainty band shown in Figure 4. The obtained confidence band for the evaluation of the

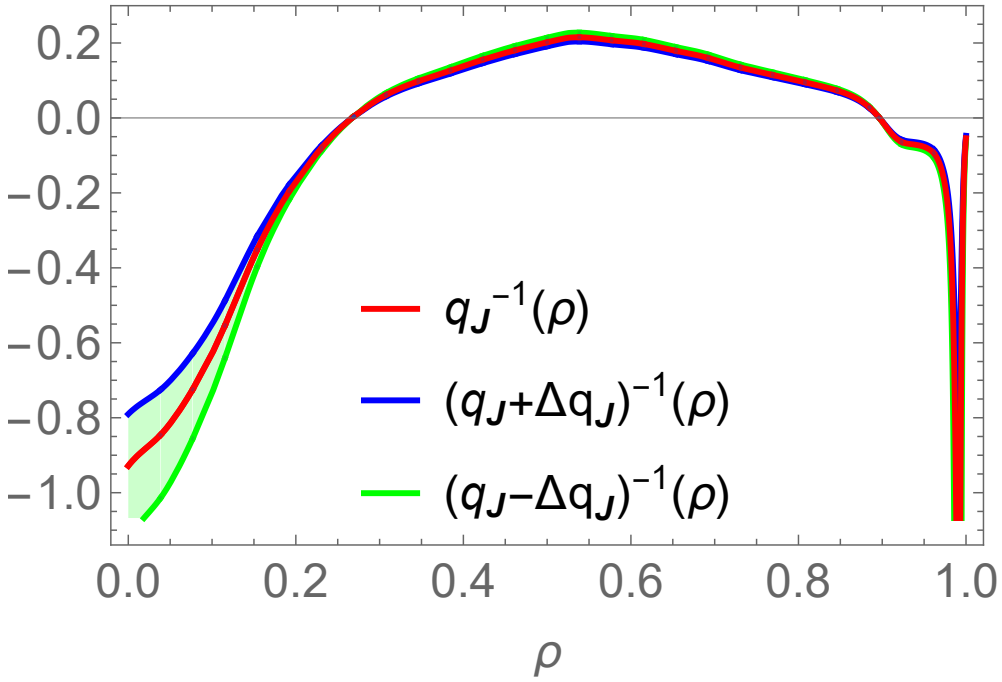

Figure 4: Evaluation of the winding profile, $q_{\mathbf{J}}^{-1}$, of the current density field lines in the QH mode. To account for the imprecision in the digitization of the $q_{\mathbf{B}}$, p' and FF' profiles and in the evaluation of the flux surface averages $\langle R^{-2} \rangle$, the confidence band for this evaluation is plotted using Eq. (8) with $\delta = 0.04$.

current density winding profile is very similar to the one plotted in Figure 3. This shows that the result obtained for $q_{\mathbf{J}}^{-1}$ is highly robust to small perturbations in the data, except in a very central zone of the tokamak plasma (roughly within $\rho < 0.15$) where its knowledge is less precise and the confidence interval is larger. The negative value of $q_{\mathbf{J}}$ in this region renders this point irrelevant in terms of the topological properties of magnetic and current density modes: in this region, irrespective of the point located within the confidence interval, filamentation modes (i.e. current density resonances) are not associated to magnetic islands but to non-resonant magnetic perturbations. Let us now delve deeper into this analysis.

4 Analysis and discussion

4.1 Classification of modes

Let us analyse the Figure 5 and consider first the current density winding profile. Any mode (m, n) such that there exists some ρ for which $q_{\mathbf{J}}(\rho) = m/n$ is resonant for the current density field, and therefore, takes the form of a current filamentation mode. This filamentation mode is, by Ampère's law, associated to some magnetic perturbation. This magnetic perturbation can be either resonant for magnetic field lines if $m/n = q_{\mathbf{B}}(\rho)$, or non-resonant otherwise. In the red stripe, the spectrum of tiny filamentation modes is associated by Ampère's law to a spectrum of non-resonant magnetic modes that has a negligible impact on electron heat transport. On the contrary, in the violet stripe, the spectrum of tiny filamentation modes is associated by Ampère's law to a spectrum of resonant magnetic modes that may impact the electron heat transport. Finally, in the blue stripe, there is no resonant mode for the current density field. Therefore, the potentially resonant magnetic modes can only arise there from smooth, non-resonant, modes of deformation of the equilibrium current density field lines.

Figure 6 shows the spatial distribution of magnetic modes, categorized according to the scheme outlined in Figure 5. The broad central region on the poloidal cross-section, depicted in blue in this figure as in Figure 5, is devoid of magnetic modes originating from the current filament spectrum. This region extends up to $\rho \approx 0.88$. This value is obtained from Fig. 5 as the ρ-value at which the function $q_{\mathbf{J}}^{-1}$ enters the violet stripe. In the outer region, depicted in violet, the resonant magnetic modes are conversely originating from a spectrum of current filamentation modes. This is due to the superposition of numerous

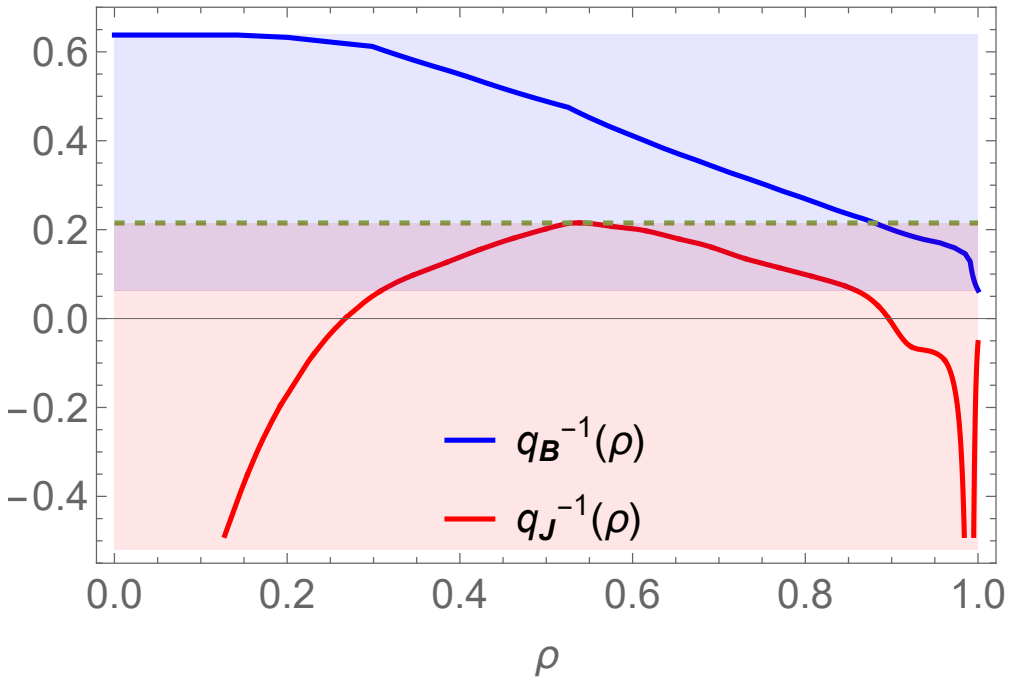

Figure 5: Plots of the winding profiles as in Figure 3. For clarity, the confidence band is not drawn. Above the horizontal dashed line, in the blue stripe, the resonant magnetic modes (m, n), such that $q_{\mathbf{B}} = m/n$ are not associated with resonant current density modes. In the violet stripe, modes are both resonant to **B** and **J**. In the red band, modes are only resonant to **J**.

current filaments that permeate the plasma in the region spanning from $\rho \approx 0.32$ to $\rho \approx 0.85$ where the image of $q_{\mathbf{J}}^{-1}$ is in the violet stripe in Fig. 5.

Consequently, the comparison of the $q = q_{\mathbf{B}}$ and $q_{\mathbf{J}}$ profiles (or, equivalently, of their inverses), in an example of QH-mode occurrence, uncovers a key feature. It reveals the existence of two distinct plasma zones: a central region unaffected by magnetic turbulence caused by current filaments, and a thin peripheral zone where there exists a spectrum of magnetic modes associated to current filaments. Let us now briefly review some experimental facts about QH-modes before interpreting this result.

4.2 Overview of QH-mode phenomenology

In the standard H-modes, ELMs result in substantial transient spikes of particle and heat fluxes to the divertor components, which could potentially cause unacceptable damage in future fusion devices. In QH-modes, the plasma remains stable and quiet, without the deleterious ELM events. In terms of confinement, QH modes are similar to H modes. Their performance indicators are at the same level. Furthermore, although the quiescent H-modes do not experience ELMs, the edge particle transport in QH-mode is still rapid enough to provide some beneficial particle exhaust, which is a crucial requirement for future fusion reactors in order to remove impurities and helium ash. The QH-mode differs then from the standard ELM-free H-mode, where the density and radiated power exhibit a monotonic increase. An edge electromagnetic mode, the edge harmonic oscillation (EHO), provides enhanced edge particle transport that, when time-averaged, surpasses the transport produced by ELMs. This allows for the constant density operation observed in the QH mode [42]. Notably, the EHO is self-generated by the plasma, and therefore the QH mode does not require the additional coils needed for ELM suppression via resonant magnetic perturbations.

4.3 Discussion

Small 3D perturbations in the equilibrium current flow near the rational surfaces, having $q_{\mathbf{J}} = m/n$, lead to the formation of a spectrum of small current density filaments. In the phase space, these filaments take the form of current density islands in a Poincaré's plot. This spectrum of 3D current density perturbations is associated by Ampère's law to a spectrum of 3D magnetic

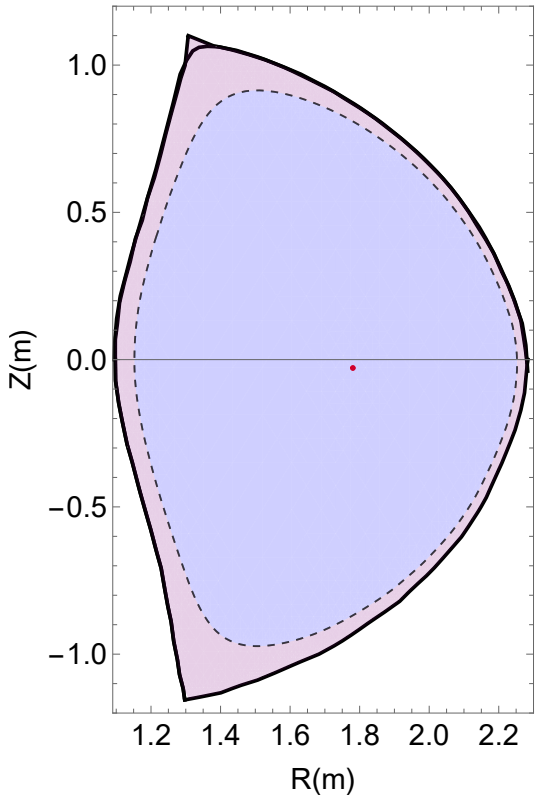

Figure 6: The large central zone colored in blue is free from resonant magnetic perturbations originating from current density filamentation modes in the QH mode. In the outer violet-colored region of the tokamak plasma having approx. $\rho > 0.88$, there exists some spectrum of resonant magnetic perturbations associated to the spectrum of tiny current filamentation modes, that are present in the interval $0.32 < \rho < 0.85$ according to Fig. 5.

perturbations. Yet, the ensuing magnetic perturbations may or may not be resonant depending on $q_{\mathbf{B}}$. In the context of the QH-mode considered here, the Figure 5 tells us that only in the violet stripe does the spectrum of tiny filamentation modes produce a spectrum of resonant magnetic perturbations triggering magnetic braiding [43]. This happens here in the edge plasma region of the tokamak represented on Figure 6. Conversely, the large central zone of the plasma, colored in blue, is preserved from this current-driven small scale magnetic turbulence. Figure 6 is therefore consistent with the phenomenological properties of QH-modes: the fact that, in the whole plasma center, the spectrum of small current density filaments does not affect the integrity of the magnetic field lines is consistent with an improved heat confinement. This makes this operating mode similar to an H-mode. Conversely, in the edge plasma, the spectrum of small current density filaments spoils the integrity of the magnetic field lines. This is consistent with a low heat and electron confinement in the edge region. This is also consistent with edge particle exhaust enabling the constant density operation in QH-mode.

In addition to these general outcomes, the present reconstruction concerns the discharge 163518 from the DIII-D tokamak at time $t = 2350$ms, where a clear EHO, a coherent edge magnetic activity characteristic of many QH-mode plasmas, with dominant $n = 1$ mode is observed. This magnetic activity can be inferred to be related to magnetic resonant modes at $q_{\mathbf{B}} = 5$ or $q_{\mathbf{B}} = 6$ having dominant mode numbers $(m, n) = (5, 1)$ or $(6, 1)$ being associated to some plasma current filamentation present at $q_{\mathbf{J}} = 5$ or $q_{\mathbf{J}} = 6$ that takes place close to $\rho = 0.55$ according to Fig. 5.

5 Conclusion

As advocated in Ref. [1], if the axisymmetric fusion device could be driven so as to disconnect $q_{\mathbf{B}}$ and $q_{\mathbf{J}}$, in the sense that the intersection of the images of the functions $q_{\mathbf{B}}$ and $q_{\mathbf{J}}$ is empty, then all the resonant magnetic modes would only originate from smooth modes of deformation of the current but not from current filament modes. All the small magnetic perturbations produced by the tiny current filaments necessarily coming in from the distorsion to axisymmetry about the resonant $q_{\mathbf{J}}$ surfaces would then not affect the integrity of the magnetic surfaces, being not resonant. Thus, by forcing the operating regime of a tokamak in such a way as to produce a pressure profile that allows the $q_{\mathbf{B}}$ and $q_{\mathbf{J}}$ profiles to be separated, the magnetic surfaces could be preserved from magnetic perturbations due to current filamentation modes. This could be a favorable route for preserving heat confinement.

This Letter presents the first cross-analysis of magnetic and current density field topologies. This uses experimental data obtained in the promising QH-mode regime. If the pattern of the magnetic and current density winding profiles displayed in Figure 5 characterizes the QH-modes, which needs further investigation, then the central region of the tokamak plasma in which $q_{\mathbf{B}}$ and $q_{\mathbf{J}}$ are disconnected supports the above scenario as heat confinement is preserved there. On the contrary, the hump in the current density winding profile taking place in the violet stripe signals that the outer plasma region is the home of a spectrum of current filament-produced resonant magnetic modes degrading the peripheral confinement. This stochastization may explain the absence of edge localized modes and allow some beneficial particle exhaust.

Overall, the present results point to a possible signature pattern of the QH-modes to be further reinforced and substantiated by additional data. Implementing the $(q_{\mathbf{B}}, q_{\mathbf{J}})$ real-time monitoring could help uncover insights into the diverse tokamak confinement regimes with possibly important implications for magnetic confinement fusion.

Acknowledments M.C.F. acknowledges support from EUROfusion H-Europe/WP24 (TRED).

References

[1] M.-C. Firpo. Interplay of the magnetic and current density field topologies in axisymmetric devices for magnetic confinement fusion. Journal of Plasma Physics (JPP) Letters, 2024. accepted on Aug 12 2024, hal-04623787.

[2] L.L. Lao, H. St. John, R.D. Stambaugh, A.G. Kellman, and W. Pfeiffer. Reconstruction of current profile parameters and plasma shapes in tokamaks. Nuclear Fusion, 25(11):1611, nov 1985.

[3] L.L. Lao, J.R. Ferron, R.J. Groebner, W. Howl, H. St. John, E.J. Strait, and T.S. Taylor. Equilibrium analysis of current profiles in tokamaks. Nuclear Fusion, 30(6):1035, jun 1990.

[4] H. Lütjens, A. Bondeson, and O. Sauter. The chease code for toroidal mhd equilibria. Computer Physics Communications, 97(3):219–260, 1996.

[5] J.R. Ferron, M.L. Walker, L.L. Lao, H.E. St. John, D.A. Humphreys, and J.A. Leuer. Real time equilibrium reconstruction for tokamak discharge control. Nuclear Fusion, 38(7):1055, jul 1998.

[6] L. L. Lao, H. E. St. John, Q. Peng, J. R. Ferron, E. J. Strait, T. S. Taylor, W. H. Meyer, C. Zhang, and K. I. You. Mhd equilibrium reconstruction in the diii-d tokamak. Fusion Science and Technology, 48(2):968–977, 2005.

[7] Jacques Blum, Cédric Boulbe, and Blaise Faugeras. REAL-TIME EQUILIBRIUM RECONSTRUCTION IN A TOKAMAK. In F.P. Orsitto, G. Gorini, E. Sindoni, and M. Tardocchi, editors, Burning Plasma Diagnostics: An International Conference, volume 988, pages p 420–429, Varenna, Italy, September 2007. American institute of physics.

[8] O. Katsuro-Hopkins, S.A. Sabbagh, J.M. Bialek, H.K. Park, J.G. Bak, J. Chung, S.H. Hahn, J.Y. Kim, M. Kwon, S.G. Lee, S.W. Yoon, K.-I. You, A.H. Glasser, and L.L. Lao. Equilibrium and global mhd stability study of kstar high beta plasmas under passive and active mode control. Nuclear Fusion, 50(2):025019, jan 2010.

[9] J. Blum, C. Boulbe, and B. Faugeras. Reconstruction of the equilibrium of the plasma in a tokamak and identification of the current density profile in real time. Journal of Computational Physics, 231(3):960–980, 2012. Special Issue: Computational Plasma Physics.

[10] G Q Li, Q L Ren, J P Qian, L L Lao, S Y Ding, Y J Chen, Z X Liu, B Lu, and Q Zang. Kinetic equilibrium reconstruction on east tokamak. Plasma Physics and Controlled Fusion, 55(12):125008, nov 2013.

[11] Blaise Faugeras, Francesco Orsitto, and JET Contributors. Equilibrium reconstruction at jet using stokes model for polarimetry. Nuclear Fusion, 58(10):106032, aug 2018.

[12] Z.A. Xing, D. Eldon, A.O. Nelson, M.A. Roelofs, W.J. Eggert, O. Izacard, A.S. Glasser, N.C. Logan, O. Meneghini, S.P. Smith, R. Nazikian, and E. Kolemen. Cake: Consistent automatic kinetic equilibrium reconstruction. Fusion Engineering and Design, 163:112163, 2021.

[13] Linjin Zheng, M. T. Kotschenreuther, F. L. Waelbroeck, and Y. Todo. ATEQ: Adaptive toroidal equilibrium code. Physics of Plasmas, 29(7):072503, 07 2022.

[14] C. Hansen, I. G. Stewart, D. Burgess, M. Pharr, S. Guizzo, F. Logak, A. O. Nelson, and C. Paz-Soldan. Tokamaker: An open-source time-dependent grad-shafranov tool for the design and modeling of axisymmetric fusion devices, 2023.

[15] Yao Huang(榛勷), Bing-Jia Xiao(鑲栴偝鑿, and Zheng-Ping Luo(缃楁　骞. Fast parallel grad-shafranov solver for real-time equilibrium reconstruction in east tokamak using graphic processing unit. Chinese Physics B, 26(8):085204, 2017.

[16] Rui MA, Fan XIA, Fei LING, and Jiaxian LI. Acceleration optimization of real-time equilibrium reconstruction for hl-2a tokamak discharge control. Plasma Science and Technology, 20(2):025601, jan 2018.

[17] Semin Joung, Jaewook Kim, Sehyun Kwak, J.G. Bak, S.G. Lee, H.S. Han, H.S. Kim, Geunho Lee, Daeho Kwon, and Y.-C. Ghim. Deep neural network grad欽撈hafranov solver constrained with measured magnetic signals. Nuclear Fusion, 60(1):016034, dec 2019.

[18] L L Lao, S Kruger, C Akcay, P Balaprakash, T A Bechtel, E Howell, J Koo, J Leddy, M Leinhauser, Y Q Liu, S Madireddy, J McClenaghan, D Orozco, A Pankin, D Schissel, S Smith, X Sun, and S Williams. Application of machine learning and artificial intelligence to extend efit equilibrium reconstruction. Plasma Physics and Controlled Fusion, 64(7):074001, jun 2022.

[19] D. A. Kaltsas and G. N. Throumoulopoulos. Neural network tokamak equilibria with incompressible flows. Physics of Plasmas, 29(2):022506, 02 2022.

[20] A Pavone, A Merlo, S Kwak, and J Svensson. Machine learning and bayesian inference in nuclear fusion research: an overview. Plasma Physics and Controlled Fusion, 65(5):053001, apr 2023.

[21] S. Douady, Y. Couder, and M. E. Brachet. Direct observation of the intermittency of intense vorticity filaments in turbulence. Phys. Rev. Lett., 67:983–986, Aug 1991.

[22] A. B. Rechester and M. N. Rosenbluth. Electron heat transport in a tokamak with destroyed magnetic surfaces. Phys. Rev. Lett., 40:38–41, Jan 1978.

[23] M B Isichenko. Effective plasma heat conductivity in 'braided' magnetic field-i. quasi-linear limit. Plasma Physics and Controlled Fusion, 33(7):795, jul 1991.

[24] M B Isichenko. Effective plasma heat conductivity in 'braided' magnetic field-ii. percolation limit. Plasma Physics and Controlled Fusion, 33(7):809, jul 1991.

[25] N. Vianello, V. Naulin, R. Schrittwieser, H. W. Müller, M. Zuin, C. Ionita, J. J. Rasmussen, F. Mehlmann, V. Rohde, R. Cavazzana, and M. Maraschek. Direct observation of current in type-i edge-localized-mode filaments on the asdex upgrade tokamak. Phys. Rev. Lett., 106:125002, Mar 2011.

[26] J. R. Harrison, G. M. Fishpool, A. J. Thornton, N. R. Walkden, and MAST team. The appearance and propagation of filaments in the private flux region in Mega Amp Spherical Tokamak. Physics of Plasmas, 22(9):092508, 09 2015.

[27] F. Ebrahimi. Nonlinear reconnecting edge localized modes in current-carrying plasmas. Physics of plasmas, 24(5), 2017.

[28] Santanu Banerjee, N. Bisai, D. Chandra, P. Dhyani, R. Manchanda, M. B. Chowdhuri, N. Ramaiya, D. Sangwan, J. Ghosh, R. L. Tanna, P. K. Chattopadhyay, D. Raju, P. K. Atrey, Y. Shankar Joisa, A. Sen, and P. K. Kaw. Observation of thick toroidal filaments during the disruptive phase of aditya tokamak plasma. Physics of plasmas, 24(10), 2017.

[29] G. Grenfell, M. Spolaore, D. Abate, L. Carraro, L. Marrelli, I. Predebon, S. Spagnolo, M. Veranda, M. Agostini, B.Ph van Milligen, R. Cavazzana, L. Cordaro, G. De Masi, P. Franz, C. Hidalgo, E. Martines, B. Momo, M.E. Puiatti, P. Scarin, N. Vianello, B. Zaniol, M. Zuin, and the RFX-mod team. Turbulent filament properties in l and h-mode regime in the rfx-mod operating as a tokamak. Nuclear fusion, 60(12):126006–, 2020.

[30] G. Z. Hao, G. Q. Dong, B. T. Cui, Y. Q. Liu, Y. H. Xu, T. F. Sun, X. Q. Ji, S. Wang, Y. F. Zhao, J. Q. Xu, X. Bai, N. Zhang, C. Y. Li, L. Wang, H. D. He, J. M. Gao, Yi Liu, W. L. Zhong, M. Xu, and X. R. Duan. Toroidal modeling of 3d perturbations generated by current filaments in scrape-off layer in tokamak with biased divertor targets. Nuclear Fusion, 63(1), 11 2022.

[31] Christopher Ham, Andrew Kirk, Stanislas Pamela, and Howard Wilson. Filamentary plasma eruptions and their control on the route to fusion energy. Nature Reviews Physics, 2(3):159–167, Mar 2020.

[32] Sarah Chouchene, Fr茅d茅ric Brochard, Nicolas Lemoine, Jordan Cavalier, Mikael Desecures, and Vladimir Weinzettl. Mutual interactions between plasma filaments in a tokamak evidenced by fast imaging and machine learning. Physical review. E, 109(4), 2024.

[33] A.Y. Pankin, J.R. King, S.E. Kruger, Xi Chen, K.H. Burrell, A.M. Garofalo, R. J. Groebner, G.R. McKee, and Z. Yan. Towards validated mhd modeling of edge harmonic oscillation in diii-d qh-mode discharges. Nuclear Fusion, 60(9):092004, jul 2020.

[34] K. H. Burrell, M. E. Austin, D. P. Brennan, J. C. DeBoo, E. J. Doyle, C. Fenzi, C. Fuchs, P. Gohil, C. M. Greenfield, R. J. Groebner, L. L. Lao, T. C. Luce, M. A. Makowski, G. R. McKee, R. A. Moyer, C. C. Petty, M. Porkolab, C. L. Rettig, T. L. Rhodes, J. C. Rost, B. W. Stallard, E. J. Strait, E. J. Synakowski, M. R. Wade, J. G. Watkins, and W. P. West. Quiescent double barrier high-confinement mode plasmas in the DIII-D tokamak. Physics of Plasmas, 8(5):2153–2162, 05 2001.

[35] K H Burrell, M E Austin, D P Brennan, J C DeBoo, E J Doyle, P Gohil, C M Greenfield, R J Groebner, L L Lao, T C Luce, M A Makowski, G R McKee, R A Moyer, T H Osborne, M Porkolab, T L Rhodes, J C Rost, M J Schaffer, B W Stallard, E J Strait, M R Wade, G Wang, J G Watkins, W P West, and L Zeng. Quiescent h-mode plasmas in the diii-d tokamak. Plasma Physics and Controlled Fusion, 44(5A):A253, apr 2002.

[36] W Suttrop, M Maraschek, G D Conway, H-U Fahrbach, G Haas, L D Horton, T Kurki-Suonio, C J Lasnier, A W Leonard, C F Maggi, H Meister, A M眉ck, R Neu, I Nunes, Th P眉tterich, M Reich, A C C Sips, and the ASDEX Upgrade Team. Elm-free stationary h-mode plasmas in the asdex upgrade tokamak. Plasma Physics and Controlled Fusion, 45(8):1399, jun 2003.

[37] W. Suttrop, V. Hyn枚nen, T. Kurki-Suonio, P.T. Lang, M. Maraschek, R. Neu, A. St盲bler, G.D. Conway, S. Hacquin, M. Kempenaars, P.J. Lomas, M.F.F. Nave, R.A. Pitts, K.-D. Zastrow, the ASDEX Upgrade team, and contributors to the JET-EFDA workprogramme. Studies of the 鈥橫uiescent h-mode鈥檈gime in asdex upgrade and jet. Nuclear Fusion, 45(7):721, jul 2005.

[38] Lorenz Meier, Matthias Hoelzl, Andres Cathey, Guido Huijsmans, Eleonora Viezzer, Mike Dunne, Jan van Dijk, Diego Jos茅 Cruz Zabala, Karl Lackner, Sibylle G盲nter, the ASDEX Upgrade Team, the EUROfusion MST1 Team, and the JOREK Team. Mhd simulations of formation, sustainment and loss of quiescent h-mode in the all-tungsten asdex upgrade. Nuclear Fusion, 63(8):086026, jul 2023.

[39] Y Sakamoto, H Shirai, T Fujita, S Ide, T Takizuka, N Oyama, and Y Kamada. Impact of toroidal rotation on elm behaviour in the h-mode on jt-60u. Plasma Physics and Controlled Fusion, 46(5A):A299, apr 2004.

[40] N. Oyama, Y. Sakamoto, A. Isayama, M. Takechi, P. Gohil, L.L. Lao, P.B. Snyder, T. Fujita, S. Ide, Y. Kamada, Y. Miura, T. Oikawa, T. Suzuki, H. Takenaga, K. Toi, and the JT-60 Team. Energy loss for grassy elms and effects of plasma rotation on the elm characteristics in jt-60u. Nuclear Fusion, 45(8):871, jul 2005.

[41] A Ya Khinchin. Mathematical foundations of statistical mechanics, Gos. Tekh. Izdat., Moscow 1943. 1949.

[42] K. H. Burrell, T. H. Osborne, P. B. Snyder, W. P. West, M. E. Fenstermacher, R. J. Groebner, P. Gohil, A. W. Leonard, and W. M. Solomon. Quiescent h-mode plasmas with strong edge rotation in the cocurrent direction. Phys. Rev. Lett., 102:155003, Apr 2009.

[43] M.-C. Firpo. Microtearing turbulence: Magnetic braiding and disruption limit. Physics of Plasmas, 22(12):122511, 12 2015.